The QSO evolution derived from the *HBQS* and other complete QSO surveys [1]

Fabio La Franca
Dipartimento di Fisica, Università degli studi "Roma TRE"
Via della Vasca Navale 84, I-00146 Roma, Italy
Electronic mail: lafranca@astrpd.pd.astro.it

and

Stefano Cristiani
Dipartimento di Astronomia, Università degli studi di Padova
Vicolo dell'Osservatorio 5, I-35122 Padova, Italy
Electronic mail: cristiani@astrpd.pd.astro.it

Submitted to the *The Astronomical Journal*

ABSTRACT

An Homogeneous Bright QSO Survey (HBQS) has been carried out in the framework of an ESO Key programme. 327 QSOs (with $M_B < -23$ and $0.3 < z < 2.2$) have been selected over an area of 555 deg^2 in the magnitude range $15 < B < 18.75$. For magnitudes brighter than $B = 16.4$ the QSO surface density turns out to be a factor 2.2 higher than what measured by the PG survey, corresponding to a surface density of $0.013^{+.007}_{-.005}$ deg^{-2}. If the data from the Edinburgh QSO Survey are included, an overdensity of a factor 2.7 is observed, corresponding to a surface density of 0.016 ± 0.005 deg^{-2}. In order to derive the QSO optical luminosity function we used Monte Carlo simulations that take into account of the selection criteria, photometric errors and QSO spectral slope distribution. We have combined our data with the Edinburgh QSO Survey, the Large Bright QSO Survey, Durham/AAT survey, ESO/AAT faint survey and the $(ZM)^2B$ survey.

The luminosity function can be represented with a Pure Luminosity Evolution, $L(z) \propto (1+z)^k$, of a two power-law both for $q_0 = 0.5$ and $q_0 = 0.1$. For $q_0 = 0.5$ the k evolution parameter is $k = 3.26 \pm 0.07$, slower than the previous Boyle's (1992) estimate $k = 3.45$. A flatter slope $\beta = -3.72 \pm 0.13$ of the bright part of the luminosity function is also required. If a spread in the QSO spectral slope of $\sigma_\gamma = 0.3$ and 0.5 is taken into account, the k parameter drops to 3.2 and 3.0 respectively. The observed overdensity of bright QSOs is concentrated at redshifts lower than 0.6. It results that in the range $0.3 < z < 0.6$ the luminosity function is flatter than observed at higher redshifts.

[1] Based on data of the ESO Key-Programme "A Homogeneous Bright QSO Survey".

In this redshift range, for $M_B < -25$, 32 QSOs are observed instead of 19 expected from our best-fit PLE model. This feature requires a luminosity dependent luminosity evolution in order to adequately represent the data in the whole $0.3 < z < 2.2$ redshift interval. The observed overdensity of low redshift bright QSOs could be originated by the contribution of a slower evolving population of radio-loud QSOs.

Subject headings: 159 - Quasi-stellar Objects

1. INTRODUCTION

The study of the evolution of the QSO Luminosity Function (LF) is of primary importance in order to understand the physic driving the central "engine" of AGNs (e.g. Efstathiou & Rees 1988, Haehnelt & Rees 1993). Studies of the large scale structure of the Universe (e.g. Andreani & Cristiani 1993), and of the extragalactic X-ray and UV background (e.g. Madau, Ghisellini & Fabian 1994; Comastri *et al.* 1995; Haardt & Madau 1996) are based on the knowledge of the optical QSO LF and its relationship with other wavebands. The LF of the optically selected QSOs is also the starting point to disentangle the evolutionary properties of the two populations of the radio-loud and radio-quiet QSOs (La Franca *et al.* 1994).

The general behaviour of the LF is fairly well established in the redshift interval $0.3 < z < 2.2$ for which color techniques provide reliable selection methods (see Hartwick and Schade (1990), Boyle (1992) and Hewett and Foltz (1994) for a review of the subject). The prevailing model was proposed by Boyle, Shanks & Peterson (1988) and was based on a sample of 420 faint ($b < 20.9$) AGNs, combined with the Palomar Green (PG) Bright QSO Sample (BQS, Schmidt & Green 1983) consisting of 92 QSOs with $B < 16.4$. The model consists of a double-power-law shape invariant with redshift, with a steep bright end $dN/dL \propto L^{-3.9}$, and a flatter faint end $dN/dL \propto L^{-1.5}$. The evolution is simply represented by the so-called Pure Luminosity Evolution (PLE) in which the characteristic luminosity (L^*) of the break between the two power-laws evolves as a function of redshift according to $L^*(z) \propto (1+z)^{3.4}$.

In the last years a number of papers have been published suggesting that the standard two power-law model in the framework of a pure luminosity evolution may not be an adequate representation of the data (Goldschmidt *et al.* 1992; Miller *et al.* 1993; Hewett, Foltz & Chaffee 1993; Hawkins & Veron 1995). The most controversial points are the amount of flattening of the faint part of the LF, first discovered by Boyle *et al.* (1988), and the shape of the bright part which, in the last decade, has been based almost entirely on the PG bright QSO survey data.

In this paper we present a new determination of the QSO LF and its evolution. We devote special care to the shape of the bright part of the LF, for which we have derived new data from a bright QSO sample: the Homogeneous Bright QSO Survey (HBQS, partly published in Cristiani *et al.* 1995). In the computation we take also into account the most relevant already existing QSO samples, in particular two new bright QSO surveys: the Edinburgh QSO Survey (EQS, Goldschmidt *et al.* 1992), and the Large Bright QSO Survey (LBQS; Hewett, Foltz & Chaffee 1995 and references therein).

2. THE SAMPLES

As discussed in section 4, we have used Monte Carlo simulations in order to derive the best fit QSO LF. For this reason our analysis is mainly based on a set of QSO samples for which the selection criteria and the photometric properties are well defined or at least can be acceptably reproduced. In addition to the knowledge of the K-correction and QSO colors, for a rigorous determination of the LF we need the definition for each sample of:

- the flux limits and selection criteria;
- the distribution of the photometric errors as a function of apparent magnitudes;
- the galactic absorption;
- the color equations of the photometric system.

The QSO LF will be computed in the Johnson B absolute magnitudes. In the following color equations the "natural" photometric systems are marked with primed letters, while the Johnson/Cousins system is represented with unprimed letters.

2.1. The HBQS

The Homogeneous Bright QSO Survey (HBQS) was started in 1989 in the framework of an ESO Key-programme. The survey covers a total of 555 deg^2 subdivided in 22 ESO/Schmidt or UKST fields at high galactic latitude around the south galactic pole ($b < -60°$).

Two Schmidt plates for each bandpass U (IIa-O + UG1 or IIIa-J + UG1), B' (IIa-O + GG385) or B_J (IIIa-J + GG395), V' (IIa-D + GG495), R (IIIa-F + RG630) or OR (IIIa-F + OG590), and I (IV-N + RG715) have been obtained at the UKST or ESO/Schmidt telescope, usually within a few months interval, in order to minimize the effects of variability. The plate material has been scanned on the COSMOS microdensitometer. The resulting tables, containing

the instrumental magnitudes and other useful parameters for the objects detected in each plate, have been merged together in one table per field. Only objects with at least 4 detections (in 10 plates) have been included in this final table. According to the ESO/UKSTU numeration, the 13 ESO fields which have been selected in the B' photometric system are: 290, 349, 355, 406, 407, 408, 410, 468, 469, 470, 474, 479, 534. The 9 UKST fields which have been selected in the B_J photometric system are: 287, 295, 296, 297, 351, 411, 413, SA94, SGP.

We have selected as candidates all the UVx "not-extremely-extended" objects satisfying a type of *modified Braccesi less-restricted* two-color criterion (La Franca, Cristiani & Barbieri 1992). The principal color for the selection has been chosen to be the $U-B'$ or the $U-B_J$ according to the type of the available plate material. The secondary color has been chosen to be B_J-R or B_J-V' or $B'-V'$, always preferring the combination giving the most reliable photometric accuracy.

The adopted color equations (Blair & Gilmore 1982) are, for the B' (IIa-O + GG385) system:

$$B = B' + 0.11(B-V);$$

while for the B'_J (IIIa-J + GG395) system:

$$B = B'_J + 0.28(B-V) \qquad (1)$$

The magnitude intervals in which the selection is virtually complete vary from field to field between $15.0 < B < 17.3$ and $15.0 < B < 18.8$. The sample extracted from these data includes 327 QSOs ($M_B < -23$, $q_0 = 0.5$, and $H_0 = 50\ Km/s/Mpc$). Cristiani *et al.* (1995) describe in detail the procedure followed in the data acquisition and reduction and report the first results obtained in six fields (~ 150 deg^2, the ones reaching fainter limiting magnitudes), providing significant statistics in the range ($16.75 < B < 18.75$).

2.2. The Edinburgh QSO Survey (EQS)

The Edinburgh bright UVx QSO Survey (EQS) has been carried out over 13 UKST fields (the area is 333 deg^2 large) with the UB_JVRI multicolor system (see Goldschmidt *et al.* 1992). The data reduction was very similar to that of the HBQS. The photometric rms errors are of 0.09 mag in each bandpass in the magnitude interval $15 < B < 18$ were most of the QSOs are. The selection criteria is fairly well represented by the equations:

$$U - B_J < -0.35 \quad and \quad B_J - R > 0.$$

The intervals of magnitude for which a reliable sample can be extracted vary from $15.0 < B < 17.5$ to $15.0 < B < 18.5$ in the different fields (Goldschmidt 1994). For our computation of the LF we have used the bright ($B < 16.5$) subsample of 8 QSOs with $z > 0.3$ published by Goldschmidt *et al.* (1992). In this subsample the AGN with $b = 15.79$ and $z = 0.380$ has been excluded because of a wrong redshift identification (Goldschmidt 1994).

2.3. The LBQS

The Large Bright QSO Survey covers an effective area of 454 deg^2 (Hewett, Foltz and Chaffee 1995 and references therein). The photometry has been carried out in the B_J bandpass and the errors are on average of 0.10 magnitudes, taking also into account zero point errors and variations across UKST fields. The sample is based on 1055 QSOs and AGNs, with apparent magnitudes in the range $16.5 < B_J < 18.85$ and redshifts in the range $0.2 < z < 3.4$. The selection has been carried using objective prism plates, looking for emission line and/or blue continuum objects. Because of the selection of the blue continuum objects the sample is complete in the redshift range $0.2 < z < 2.2$. It is not possible to directly simulate the selection criteria of this survey, however in order to check the effects in the LF by the inclusion of such a large database, we have temptatively simulated the blue continuum selection as an UVx selection:

$$U - B_J < -0.30.$$

As for the EQS and HBQS samples the adopted color equation is (1). In our computation of the LF we have restricted the LBQS to a subsample of 220 QSOs in the magnitude range $16.5 < B < 18.0$.

2.4. The SA94 Survey

The SA94 survey is an UVx (UBV) selected sample over an area of 10 deg^2. The QSOs have been selected according to the *less restricted* Braccesi UVx criterion (La Franca *et al.* 1992). The completeness magnitude range is $15.0 < B < 19.9$. The complete sample extracted from the data includes 97 QSOs. The B magnitudes are directly published in the Johnson/Cousins system and no color transformation is needed.

2.5. The Durham/AAT Survey

This sample comes from an UVx stellar object selection from UK Schmidt U and B_J plates. The B_J plates have been calibrated on the B magnitude system. Therefore the magnitudes of this surveys are referred as b magnitudes for which the color equation is (Boyle *et al.* 1990):

$$B = b + 0.23(B - V - 0.9).$$

The whole catalogue containing 420 AGNs is subdivided in 34 circular fields having a diameter of $40'$, corresponding to a total area of 11.9 deg^2. The completeness magnitude ranges vary from field to field, the faintest limit magnitude reaching $b = 20.9$. Different UVx selection limits have also been adopted in the various fields (see Boyle *et al.* 1990, Table 2). On average they correspond to $u - b < -0.40$. In the redshift interval $0.3 < z < 2.2$ the sample consists of 353 QSOs.

2.6. The ESO/AAT

This is a faint $UJRI$ survey of 66 AGNs in the fields 855, 861, 864 (Boyle, Jones and Shanks 1991), where J' is a IIIa-J + GG385 system. The color equation is (Kron 1980):

$$B = J' + 0.23(B - V).$$

The survey covers an effective area of 0.85 deg^2 from $J = 18.0$ down to $J = 21.75 - 22.0$, and the completeness redshift range is $0.6 < z < 2.9$. The typical rms scatter in the calibration is 0.09 mag for the J bandpass, 0.15 mag for R passband, and 0.12 mag in the U bandpass. The candidates were selected among all the stellar objects lying blueward of the stellar locus in either $U - J$ or $J - R$ diagrams. At $z < 2.2$ the subsample consists of 41 QSOs whose selection is well represented with

$$U - J < -0.30.$$

2.7. The (ZM)^{2}B Survey

This is a faint UVX survey of 54 AGNs from UJF plates taken at the ESO 3.6m telescope (Zitelli *et al.* 1992). The survey cover an area of 0.69 deg^2 down to $J = 20.85$ and 0.35 deg^2 down to $J = 22.0$. In the redshift range $0.3 < z < 2.2$ the complete sample consists of 19 QSOs. The selection criterion is well represented by

$$U - J < -0.30.$$

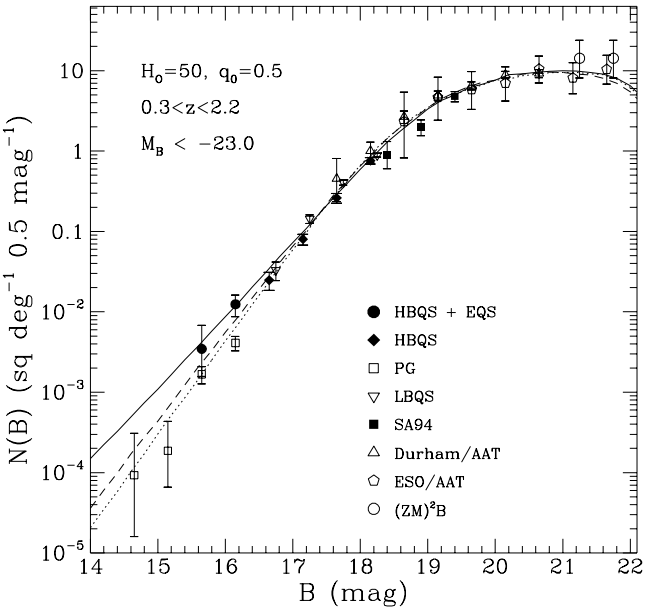

Fig. 1.— The QSO number counts for $0.3 < z < 2.2$. The continuous line represents the best fit LDLE model (model C in Table 2), the dashed line represents our best fit PLE model (model B in Table 2), while the dotted line represents the best fit PLE model (model A in Table 2) by Boyle *et al.* (1992). The magnitudes have all been corrected for galactic extinction according to Burstein and Heiles (1982).

As in the previous survey the color equation is:

$$B = J' + 0.23(B - V).$$

3. THE QSO COUNTS

The B number-magnitude counts for all the samples used in the computation of the optical LF are shown in Fig. 1. In the following we will restrict our analysis to $0.3 < z < 2.2$ because this is the only interval in which the selection criteria allow a reliable and homogeneous processing of the data. The magnitudes have all been corrected for galactic extinction according to Burstein & Heiles (1982). The QSO surface densities from the HBQS and EQS are also shown in Table 1. As first indicated by Goldschmidt *et al.* (1992), for magnitudes brighter than $B = 16.4$ the QSO surface density turns out to be a factor 2.5 higher than what measured by the PG survey (Schmidt & Green 1983).

The data from the HBQS collect 7 QSOs at magnitudes brighter than $B = 16.4$, corresponding to a surface density of $0.013^{+.007}_{-.005}$ deg^{-2}. With the addition of the EQS, the surface density at $B < 16.4$ becomes 0.016 ± 0.005 deg^{-2}, corresponding to a total of 14 QSOs over an area of 888 deg^2. The PG sample lists 44 QSOs at $B < 16.4$. In this range the surveyed area changes rapidly as a function of the limiting magnitude. Combining the number of discovered QSOs with the areas according to Table 1 of Green, Schmidt & Liebert (1986), a QSO surface density of 0.006 ± 0.001 deg^{-1} is obtained, a factor of 2.7 lower (significant at 2σ level) than the EQS+HBQS estimate. The presence of incompleteness in the PG survey has been investigated by Wampler and Ponz (1985). It probably originates for QSOs with $U - B$ colors near the selection limit because of large rms errors. This effect would lead to incompleteness that varies with redshift, with the consequence that, in particular in the range $0.4 < z < 0.7$, it is systematically underpopulated at a given magnitude. This hypothesis appears corroborated by the fact that the PG survey, in the area covered to a limit $B = 16.4$, has discovered 46 QSOs with $z < 0.3$, in addition to the 44 with $z > 0.3$ that are relevant for the comparison with the current sample. For these reasons we have excluded the PG sample from our subsequent analysis of the evolution of the LF. At fainter magnitudes, in the interval $16.5 < B < 18.5$, the HBQS shows a fairly good agreement with the counts of the LBQS.

4. THE LUMINOSITY FUNCTION

4.1. Deterministic Derivations

The QSO LF $\Phi(M, z)$ is the measure of the number of QSOs per unit of commoving volume with magnitudes in the interval $(M, M + dM)$ as a function of redshift z. In the redshift interval $0.3 < z < 2.2$ the general behaviour of the QSO LF has been usually parameterized with a double power-law Pure Luminosity Evolution (PLE) model $\Phi(M_B, z) =$

$$\frac{\Phi^*}{10^{0.4[M_B - M_B(z)](\alpha+1)} + 10^{0.4[M_B - M_B(z)](\beta+1)}}$$

where α and β correspond to the faint-end and bright-end slopes of the optical LF, respectively. With this parameterization the evolution of the LF is uniquely specified by the redshift dependence of the break magnitude,

$$M_B(z) = M_B^* - 2.5k \log(1 + z),$$

corresponding to a power-law evolution in the optical luminosity, $L^* \propto (1 + z)^k$. $\Phi(M_B, z)$ is expressed in units of $Mpc^{-3}mag^{-1}$ (see Boyle *et al.* 1988).

The empirical way of deriving the LF is by collecting all the available QSO samples, computing the transformations to a common photometric bandpass, and measuring the QSO space densities in Δz, ΔM bins using the $1/V_a$ estimator of the "coherent" method of Avni & Bahcall (1980); where V_a is the *accessible volume* computed for every object over all the samples and not just the sample in which the object originated. This method has a number of disadvantages as it is affected by:

1. the uncertainties due to the binning of the data. As the number of QSOs in the available complete samples is still small, it is necessary to use relatively large bin sizes on the $M_B - z$ plane within which the evolutionary effects are not negligible. In this way the non-linear dependencies of the QSO LF on M_B and z cause spurious trends on the derived shape of the LF.

2. the influence of the photometric errors. Cavaliere, Giallongo and Vagnetti (1989) pointed out how the uncertainties introduced in the statistical samples of QSOs by photometric variances and from the fluctuation of the sky variations cause an overestimation of the evolution timescales (see also Giallongo and Vagnetti 1992, and Francis 1993).

3. the spread in the assumed mean spectral index of the QSOs used to compute the K-correction. If the contribution of the emission lines to the broadband flux can be neglected, the formula relating the absolute and apparent blue magnitudes is (Schmidt & Green 1983) $M_B =$

   $$B - 5 \log[A(z)c/H_0] + 2.5(1 + \gamma) \log(1 + z) - 25,$$

   where $A(z)c/H_0$ is the bolometric luminosity distance, and the extrapolation from the observed to the rest-frame B band assumes a power-law representation of the QSO continuum $f_\nu \propto \nu^{-\gamma}$. When quantifying the evolution of the population between two redshifts,

if the extrapolation is large, it is important to know the spread of the distribution of γ. Any distribution of the mean spectral index is reflected in an uncertainty in the absolute magnitudes, which increases with redshift and introduces an artificial luminosity evolution of the population. The dispersion in the power-law index γ in the rest-frame ultraviolet is substantial (Sargent, Steidel and Boksenberg 1989; Francis *et al.* 1991; Schneider *et al.* 1991), with estimates of $\sigma_\gamma = 0.3 - 0.6$. For a sample of QSOs measured at the same observed wavelength the differential effect between two redshifts z_1, z_2 is

$$\Delta M_B = 2.5\Delta\gamma \log[(1+z_2)/(1+z_1)].$$

In the redshift range of our analysis $0.3 < z < 2.2$, changing from $z = 0.3$ to $z = 2.2$ results in a uncertainty $\sigma_{M_B} \simeq \sigma_\gamma$. A value $\Delta\gamma = 0.5$ would correspond to an error in the space density of a factor 3 in the bright part of the LF assuming a power-law index $\beta = -3.5$. In the case of two QSOs of the same redshift and apparent magnitude B but different spectral index, the difference in absolute magnitude is

$$\Delta M_B = 2.5\Delta\gamma \log(1+z).$$

Changing from $\gamma = 0$ to $\gamma = 1.5$ would produce at $z = 0.4$ a difference in absolute magnitude of $\Delta M_B = 0.4$ mag. At $z = 2.2$ the difference becomes 1.9 mag corresponding to an error in the space density of a factor 100 in the bright part of the LF (assuming a power law index $\beta = -3.5$). The final result of this effect is a blurring of the LF.

The "standard" maximum likelihood techniques (Marshall *et al.* 1983, Boyle, Shanks and Peterson 1988) do not need binning of the data and overcome the disadvantage described in item (1), but do not solve problems (2) and (3).

In order to take into account also these latter two effects, it has been proposed to compute a detection probability as a function of apparent magnitude, redshift and Spectral Energy Distribution (SED) (see Warren, Hewett & Osmer 1994). The detection probability $p(m, z, SED)$ is derived computing the fraction of QSOs that would have been selected by each survey according to the selection criteria, photometric errors, and the spectral index. Thus, for each redshift and magnitude interval, the space density is evaluated as $\Sigma 1/\int p(z)dV_a$. Eventually, in order to determine the range of parametric luminosity-function models that are consistent to the data, the observed and expected number of QSOs are compared through maximum likelihood or least χ^2 techniques.

4.2. The Monte Carlo Simulations

The above described procedures do not lead to a fully satisfactory and rigorous determination of the LF. The photometric errors and the spread in the QSO SED properties make the nature of the problem intrinsically stochastic. Even taking into account the influence of different SEDs in the computation of the absolute luminosity, the problem remains basically unsolved. For example, because of the effects of the photometric errors, two QSOs observed at the same apparent magnitude and with the same SED and redshift may be produced by objects of different absolute magnitudes. This means that it is impossible to establish a bi-unique (one-to-one) relationship between the observed apparent magnitudes and the absolute magnitudes as a function of z and SED.

For these reasons we have followed a different approach, simulating, with Monte Carlo techniques, what happens when a selection of a sample is made. For each sample the following procedure has been applied:

1. Assuming a theoretical LF distribution $\Phi(M_B, z)$, a number (proportional to the surface area of the survey) of QSOs (i.e. pairs M_B, z) have been randomly extracted;

2. The apparent magnitudes of the QSOs have been computed following the K-correction according to Cristiani & Vio (1990), and deriving the average galactic absorption A_B from the HI maps of Burstein and Heiles (1982). The resulting apparent B magnitude is:

   $$B = M_B + 5\log[A(z)c/H_0] + 25 + K(z) + A_B + \epsilon(B)$$

   where $\epsilon(B)$ simulates a noise with Gaussian distribution with variance

   $$\sigma_B^2 = \sigma_{phot}^2(B) + \sigma_{B,\gamma}^2.$$

   σ_B^2 takes into account both the photometric errors of the survey $\sigma_{phot}(B)$ and the apparent

magnitude dispersion due to the QSO spectral slope dispersion σ_γ

$$\sigma_{B,\gamma} = 2.5\sigma_\gamma \log(1+z).$$

3. The apparent colors have been generated following the average QSO colors-redshift dependence $F_{1,2}(z)$ (Cristiani & Vio 1990). Between each couple of bandpasses centered at λ_1 and λ_2 the resulting apparent color is:

$$C_{1,2} = F_{1,2}(z) + \epsilon_{F_{1,2}}$$

where $\epsilon_{F_{1,2}}$ simulates a noise with Gaussian distribution with variance

$$\sigma^2_{F_{1,2}} = \sigma^2_1 + \sigma^2_2 + \sigma^2_{F,\gamma}.$$

$\sigma^2_{F_{1,2}}$ takes into account the photometric errors of the two bandpass σ_1 and σ_2 respectively, and the QSO color dispersion due to the spread σ_γ in the slope of the spectra

$$\sigma_{F,\gamma} = 2.5\sigma_\gamma \log\frac{\lambda_2}{\lambda_1}.$$

Note that the error on the color $\sigma_{F,\gamma}$ is correlated with the error on the apparent magnitude $\sigma_{B,\gamma}$. For each simulated QSO the same value of γ has been used to compute the apparent magnitude and colors.

4. The flux limits and selection criteria of the survey have been applied to the resulting magnitudes and colors in order to select the "observed" QSOs.

In addition to statistical errors, the presence of systematic errors in the QSO photometry could induce biases in the Monte Carlo simulations. In particular the applicability of the Blair and Gilmore (1982) transformations, which have been calibrated on a range of colors ($-0.4 \leq U-B \leq 2.0$), not entirely relevant for low-redshift QSOs, is not straightforward. It is reassuring that the object for which the effect might be significant for the selection/non-selection, are those closer to the stellar locus, where the color transformations are still reliable.

The observed QSO magnitudes and colors are also affected by variability that in principle gives origin to at least two effects:

1. The shape of the LF is modified (blurred) by variability. We will derive the QSO LF as it is observed at a given instant, so we will neglect the effect from this point of view. How such a "snapshot" LF is translated into an "average" LF, describing the distribution of the average luminosities of QSOs on long timescales, is matter for future variability studies.

2. Variability is going to affect the observed colors of QSOs, acting as an additional photometric error, if the photometric material in the different colours is obtained at different times. The critical timescale above which the effects of variability become non-negligible can be set at about one year in the observer's rest frame (Cristiani *et al.* 1996). However, the effects of variability can be modeled with a spectral slope variable in time. In particular this can reproduce the observed dependence of the variability on the wavelength (Di Clemente *et al.* 1996, Cristiani *et al.* 1996). In this a variable spectral slope could manifest itself in an ensemble of QSOs as a spread in the observed spectral index, that is already included in our computations. Therefore we have not introduced further effects of the variability on the spread of the QSO colors.

4.3. Results

As discussed in section 2, in order to compute the best fit LF we have added the QSOs of the HBQS and EQS to all the optically selected samples for which it was possible a reliable assessment of the selection criteria and the photometric quality. In this way, a total sample of 1022 QSOs has been obtained. The fits have been carried out by minimizing the χ^2 statistics derived from the comparison of the observed (B, z) distribution with 2000 simulations of each theoretical LF model. Table 2 summarizes the results for a number of different models.

The errors quoted for the parameters are 68 per cent (1 σ) confidence intervals. They correspond to variations of $\Delta\chi^2 = 1.0$, obtained perturbating each parameter in turn with respect to its best-fit value, and looking for a minimization with the remaining parameters free to float.

The significance of the fitting has also been tested for goodness-of-fit in the lowest redshift interval $0.3 < z < 0.6$, in which the fitting probabilities have been computed using the two-dimensional Kolmogorov-

Smirnov (2D KS) test by Fasano and Franceschini (1988). See Press *et al.* (1992) for a complete description of the algorithm.

In the following we first focus our discussion on a $q_o = 0.5$ universe, we will later see how our results change for $q_o = 0.1$.

In Fig. 2 our best fit PLE model (B) is shown. The data points, representing the estimates of the QSO space densities, are compared to the fitted LF. The observed QSO space densities have not been directly computed through the $1/V_a$ technique, that, due to the binning of the data, can give origin to spurious trends on the shape of the LF (see sub-section 4.1). For this reason we have preferred to exploit our Monte Carlo simulation code in order to *visualize* the LF. The value of each observational point in Fig. 2 has been computed by comparing, in each absolute magnitude/redshift bin, the number of observed QSOs, N_o, with the number of QSOs simulated with the fitting LF, N_s. Let us call Φ_o and Φ_s the corresponding luminosity functions and $\Psi(M, z)$ the selection function. In each bin we have:

$$\frac{N_o}{N_s} = \frac{\int \Psi(M,z)\Phi_o(M,z)dMdz}{\int \Psi(M,z)\Phi_s(M,z)dMdz},$$

where the integrals are computed over the corresponding bin. In our case, *in each bin*, we can assume that the shape of the observed and fitting LFs are very similar, apart from a constant factor k, which varies from bin to bin: $\Phi_s \simeq k\Phi_o$. Using this assumption we can write:

$$\frac{N_o}{N_s} \simeq \frac{\Phi_o(M,z)}{\Phi_s(M,z)},$$

for all values M and z in the bin. Consequently, for proper visualization of the data, the observed QSO densities have been computed by multiplying the corresponding value of the simulating LF, Φ_s, at the central magnitude and redshift of the bin, by the ratio between the number of observed and simulated QSOs in the corresponding bin:

$$\Phi_o(M,z) \simeq \frac{N_o}{N_s}\Phi_s(M,z).$$

The 1 σ upper and lower limits have been estimated with the Poissonian statistics uncertainties on N_o. As described above, the LF fitting technique is completely independent from these assumptions, being based on a χ^2 minimization of the difference between N_o and N_s in bins of B and z.

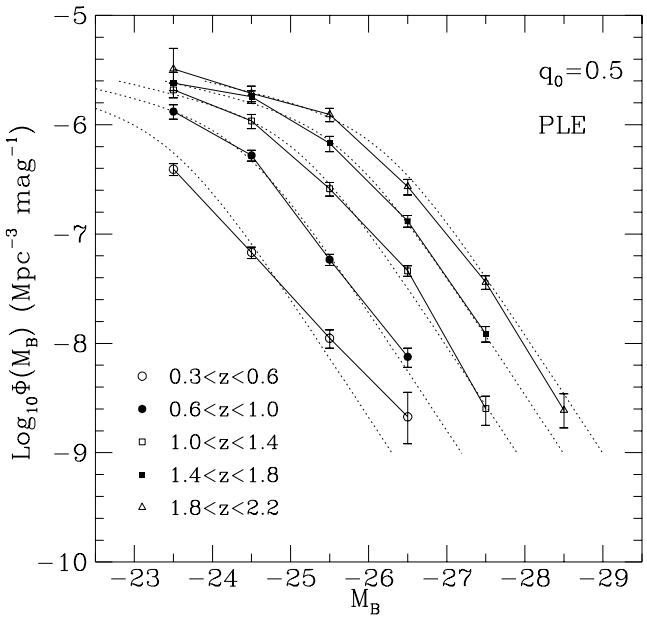

Fig. 2.— The QSO luminosity function. The points connected with a continuous line represent the observations (see text for details about their derivation). The dashed lines correspond to the best-fitting Pure Luminosity Evolution (model B in Table 2). Error bars are based on Poisson statistic and correspond to 68 per cent (1σ) confidence intervals.

Our PLE model B gives a satisfactory fit of the (B, z) distribution with a global χ^2 probability of 0.21. The PLE model A by Boyle (1992), compared with the present data, provides a lower but still acceptable probability of 0.12, however with one additional parameter, $z_{cut} = 1.9$, representing the redshift at which the luminosity evolution "switches off". At redshift greater than z_{cut} no further luminosity evolution takes place. Our B model has a flatter bright slope β (-3.7 compared to -3.9) than the A model. The evolution parameter k is also smaller (3.26 compared to 3.45).

This difference in the parameter β is originated by a larger density of luminous QSOs (expecially at $z < 0.6$) in comparison with the previous data derived from the PG sample (compare Fig. 2 with Fig. 3b of Boyle 1992). The higher evolutionary rate k deter-

mined by Boyle (1992) is a result of the introduction of the redshift cut off at $z_{cut} = 1.9$, which with our data results unnecessary.

Both A and B models provide an inadequate simulation of the distributions of the observed data for the low redshift domain, $0.3 < z < 0.6$. For this subsample the 2D KS statistics test rejects model A at the 0.01 level and model B at 0.02 level. At magnitudes brighter than $M_B = -25$, in the interval $0.3 < z < 0.6$, 32 QSOs are observed, while 16 and 19 QSOs are predicted by model A (a 4 σ discrepancy) and B (a 3 σ discrepancy) respectively. But as the low redshift ($z < 0.6$) subsample contain only 5 per cent of the complete data set, in a global comparison of the whole data sample in the interval $0.3 < z < 2.2$, the models follow the evolution of the larger fraction of QSOs at higher redshift, allowing the χ^2 probability of the global fit to reach satisfactory levels.

No significant difference is obtained by fitting the data excluding each of the three bright samples (HBQS, EQS and LBQS) in turn (models D, E and F).

It is interesting to see how the inclusion of a spread in the theoretical average QSO spectral slope modifies the best fit luminosity function. As expected (Giallongo and Vagnetti 1992), larger values of the spread of the slope correspond to slower luminosity evolution parameters and steeper luminosity functions (model G with $\sigma_\gamma = 0.3$, and model H with $\sigma_\gamma = 0.5$).

In order to fully represent the data in the redshift range $0.3 < z < 2.2$ we tried several functional modifications of the PLE. As first step we tried, without significant results, to add one or at maximum two parameters in order to take into account of a dependence of the bright slope β with redshift.

The best description of the observed data has been obtained by decreasing at low redshift the luminosity evolution of the bright QSOs. This has been obtained by including a dependence on the redshift and absolute magnitude of the evolution parameter k such as:

$$\begin{aligned} for\ M_B \le M^* \quad &: \quad k = k_1 + k_2(M_B - M^*)e^{-z/.49} \\ for\ M_B > M^* \quad &: \quad k = k_1 \end{aligned} \tag{2}$$

where M^* is the magnitude of the break in the two power-law shape of the LF. This luminosity dependent luminosity evolution (LDLE) model (model C in Table 1) has resulted in a better fit of the data (see Fig. 3) giving a χ^2 test probability of 0.49 in the whole B, z plane, and an acceptable 2D KS probability of 0.09 in the redshift interval $0.3 < z < 0.6$.

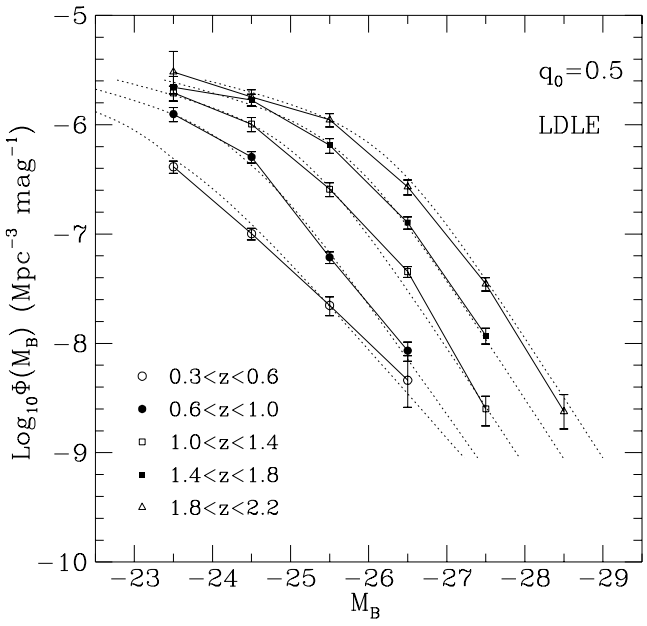

Fig. 3.— The QSO luminosity function. The points connected with a continuous line represent the observations (see text for details about their derivation). The dashed lines correspond to the best-fitting Luminosity Dependent Luminosity Evolution (model C in Table 2). Error bars as in Fig. 2.

With this model, in this redshift interval and for magnitudes brighter than $M_B = -25$, 29 QSOs are expected in comparison with the 32 observed.

In this way, as shown in Fig. 1, the LDLE reproduce the higher counts of bright QSOs at $B < 16.4$, discovered by the HBQS and EQS surveys, much better than the PLE models: a surface density of 0.017 deg^{-2} is predicted with respect to 0.016 deg^{-2} observed. The A model by Boyle (1992) predicts a surface density of 0.008 deg^{-2}.

It is important to notice that both the PLE and the LDLE models do not reproduce a 2σ significant observed underdensity of faint QSOs ($-23 > M_B > -25$) in the redshift range $0.3 < z < 0.6$. In this bin, with the PLE B model, 125 QSOs are observed and 161 expected. It is possible to find less significant indications of this feature in the data analyzed by Boyle (1992). We examined the possibility that this observed underdensity of the faint part of the luminosity function at low redshift is due to an underes-

timated incompleteness of the UVx optical selection method at low redshift. For this reason we have carried out simulations assuming a redder $U-B$ QSO color of 0.2 magnitudes in the interval $0.3 < z < 0.8$. The effects were still insufficient to account for the underdensity at low redshift (125 QSOs observed and 154 expected). As our best fit probabilities are satisfactory, we preferred not to model the low redshift faint feature. It is worth to notice that the determination of the local ($z = 0$) AGN (Seyfert 1 plus QSOs) LF from the Hamburgh Bright QSO Survey (Wisotzki *et al.* 1996a) shows similar trends, with evidences of higher densities at bright magnitudes and lower densities at faint magnitudes in comparison with the de-evolved PLE LF by Boyle (1992) (Wisotzki *et al.* 1996b; Köhler 1996).

Adopting a $q_o = 0.1$ Universe, as shown in Table 2, the fitting of the data with the PLE model (I) by Boyle (1992) is rejected at 0.004 confidence level. Our PLE model (L) obtains an acceptable global representation of the data (χ^2 probability 0.36), slightly better than the PLE fit in a $q_o = 0.5$ Universe. However, in the $0.3 < z < 0.6$ redshift range the PLE still underestimates the expected number of QSOs, although the discrepancy is less serious than in the $q_o = 0.5$ case: 44 QSOs with $M_B < -25$ are observed versus 33 predicted in our L model (24 in the I model). The introduction of a LDLE parameterization according to Eq. 2 provides satisfactory representation of the observations in the low-z domain also for $q_o = 0.1$.

5. DISCUSSION

What is the origin of the flattening of the luminosity function at low-redshift and is it confirmed by observations in other wavebands?

In the last years evidence has been produced that optically selected QSOs have a bimodal distribution of radio flux densities, and that the fraction of radio loud QSOs decreases with increasing redshift and decreasing absolute optical luminosity (Miller *et al.* 1990; Visnovsky *et al.* 1992; Schneider *et al.* 1992; Padovani 1993; La Franca *et al.* 1994).

La Franca *et al.* (1994) have determined that the radio-loud fraction is substantially higher for QSOs with $z < 1$, a result essentially due to the higher overall radio-loud fraction in the predominantly low redshift PG sample. The radio-loud fraction has also been found to be larger at bright absolute magnitudes, regardless of whether or not the PG sample is included in the analysis. La Franca *et al.* (1994) have been able to reproduce the data with a radio-loud optical luminosity function (OLF) characterized by a lower space density, a similar shape and a smaller evolutionary parameter k ($2.7 < k < 3.1$) with respect to the parent *total* (radio-quiet plus radio-loud) QSO population. According to this picture the flattening of the bright part of the OLF corresponds to an increase of the radio-loud OLF contribution.

However, the decrement of the radio-loud fraction with redshift relies essentially on the PG sample and has not been confirmed by a study of 256 QSOs in the LBQS (Hooper *et al.* 1995). Nevertheless there is a very small overlap in the magnitude redshift plane between the LBQS and the PG sample: the LBQS QSOs are too faint and too high-redshift to be compared with the PGs. Our observed overdensity of low redshift ($0.3 < z < 0.6$) QSOs involves the QSOs with $B < 16.5$ and $M_B < -25$ but in the LBQS there are only two such QSOs with $B < 16.5$, to be compared with the 45 QSOs of the PG sample. In the EQS plus HBQS combined sample there are 16 QSO brighter than 16.5. It becomes crucial to obtain radio data of this QSO subsample.

Other information on the evolution of the LF and on the dependence of the radio loud fraction on magnitude and redshift can be derived from QSO samples selected in the soft X-rays.

A study of the EMSS AGN sample by Maccacaro *et al.* (1991) and Della Ceca *et al.* (1992) has shown that a PLE model with a power-law dependence on the redshift, $L_x(z) = L_x(0)(1+z)^k$, provides the simplest description of data. Their best-fitting evolution rate ($k_x = 2.56$) is almost one unit lower than the optical best fit. Boyle *et al.* (1993) used a new sample of faint AGNs selected by ROSAT, combined with the EMSS sample, to derive a value of $k = 2.8$. Using the same data Franceschini *et al.* (1994) showed that the evolution rate of X-ray selected AGNs could have been underestimated and actually be comparable to that of the QSOs in the optical, with a linear scaling of the emission in the two bands. Boyle *et al.* (1994) using an enlarged sample of 107 faint AGNs selected by ROSAT, combined with EMSS sample, derived an evolution $L_x(z) = L_x(0)(1+z)^{3.25}$ at $z < 1.6$, quite similar to that of optically selected QSOs. The latter two analyses favour a picture in which the same QSO population is observed, both in the soft-X and in the optical. If this is true, at low z, bright X-ray selected samples should show a flattening of the

bright part of the OLF and an increase of the radio loud fraction. Unfortunately the brightest X-ray selected QSO sample, the EMSS, is not bright (large) enough to probe this domain of the OLF. In the interval $0.1765 < z < 0.4286$ the brightest significant bin is at $LogL_X = 45\ ergs^{-1}$ $(0.3 - 3.5\ KeV)$ (Maccacaro *et al.* 1991), which corresponds to about $M_B = -25$ ($q_0 = 0.1$, see Fig. 5 in Franceschini *et al.* 1994, and La Franca *et al.* 1995), in the interval $0.4286 < z < 08182$ the EMSS reaches $LogL_X = 45.5\ ergs^{-1}$ $(0.3 - 3.5\ KeV)$, corresponding to about $M_B = -26$. It is interesting to notice that Jones *et al.* (1996), at bright magnitudes in the interval $0.0 < z < 0.4$, show a flatter X-ray LF with respect to their PLE model (see their Figure 5).

Della Ceca *et al.* (1994) have analyzed the radio properties of the EMSS: they find that in a subsample of optically luminous QSOs, 30% of the objects are radio-loud, while in the complementary faint subsample the fraction of radio-loud drops to 3%. No evidences are found that the evolutionary properties of the radio-loud objects differ significantly from the radio-quiet ones. However, the shape of the deevolved XLF of the two classes appears to be different and a flattening of the XLF of the radio-loud subsample is visible for $L_X(z = 0) < 3 \times 10^{44}\ ergs^{-1}$.

Ciliegi *et al.* (1995) have obtained VLA observation of a ROSAT sample of 80 faint AGNs. They combined their sample with EMSS data and found that, in the case of a PLE, $L_x(z) = L_x(0)(1 + z)^k$, $k = 2.43 \pm 0.26$ and $k = 2.71 \pm 0.10$ for the radio-loud and radio-quiet population respectively. Although not significant, the difference hints a slower evolution of the radio loud population.

In summary, at the moment data from different wavebands suggest that:

1. There is a flattening of the bright part of the OLF at low redshift;
2. There is an increase of the radio-loud fraction at $M_B < -25$ both in X-ray and optically selected samples;
3. The apparent luminosity evolution of the radio-loud population is slower both in optically and in X-ray selected samples;
4. The same QSO population is selected in the optical and soft-X domains, and X-ray selected QSOs follow a PLE evolution similar or slower than that of the optically selected QSOs;
5. The X-ray selected samples do not have a sufficient coverage of the L, z plane to allow a meaningful cross-check of the flattening in the bright part of the low-z OLF.

In this way the observed overdensity of low redshift bright QSOs and the related flattening of the LF could be originated by the contribution of a slower evolving population of radio-loud QSOs. To put this scenario on a firmer basis it is necessary to obtain radio data for: 1) a new bright, wide field ($\sim 10000\ deg^2$) QSO sample, in the interval $13 < B < 16$, and 2) a wide field bright X-ray selected QSO sample. The former will be provided by the Sloan Survey (Gunn and Weinberg 1995), while the Rosat All Sky Survey seems to be ideally tailored for the latter.

6. acknowledgements

FLF acknowledges financial support from CNR, the hospitality of the *Dipartimento di Astronomia dell'Università di Padova*, and of the *Istituto di Astronomia dell'Università "La Sapienza" di Roma*. This work was partially supported by the ASI contracts 92-RS-102, 94-RS-107 and 95-RS-38 and by the HCM programme of the European Community.

REFERENCES

Andreani S., Cristiani S. 1992, ApJ, 298, L13

Avni Y., Bahcall J.N. 1980, ApJ, 235, 694

Blair M., Gilmore G. 1982, PASP, 94, 742

Boyle B.J., Shanks T., Peterson B.A. 1988, MNRAS, 235, 935

Boyle B.J., Fong R., Shanks T., Peterson B.A. 1990, MNRAS, 243, 1

Boyle B.J., Jones L.R., Shanks T. 1991, MNRAS, 251, 482

Boyle B.J. 1992, in "Texas/ESO-CERN Symposium on Relativistic Astrophysics, Cosmology and Particle Physics", ed(s) Barrow J.D., Mestel L. and Thomas P., Ann. N.Y. Acad. of Sci., 647, 14

Boyle B.J., Griffiths R.E., Shanks T., Stewart G.C., Georgantopoulos I. 1993, MNRAS, 260, 49

Boyle B.J., Shanks T., Georgantopoulos I., Stewart G.C., Griffiths R.E. 1994, MNRAS, 271, 639

Burstein D., Heiles C. 1982, AJ, 87, 1165

Cavaliere A., Giallongo E., Vagnetti F. 1989, AJ, 97, 336

Ciliegi P., Elvis M., Wilkes B.J., Boyle B.J., McMahon R.G., Maccacaro T. 1996, MNRAS, 277, 1463

Comastri A., Setti G., Zamorani G., Hasinger G. 1995, A&A, 296, 1

Cristiani S., Vio R. 1990, A&A, 227, 385

Cristiani S., La Franca F., Andreani, P., *et al.* 1995, A&AS, 112, 347

Cristiani S., Trentini S., La Franca F., Aretxaga I., Andreani P., Vio R., Gemmo A. 1996, A&A, 306, 395

Della Ceca R., Maccacaro T., Gioia I.M., Wolter A., Stocke J.T. 1992, ApJ, 389, 491

Della Ceca R., Zamorani G., Maccacaro T., Wolter A., Griffiths R., Stocke J.T., Setti G. 1994, ApJ, 430, 533

Di Clemente A., Giallongo E., Natali G., Trevese D., Vagnetti F. 1996, ApJ, 463, 466

Efstathiou G., Rees M.J. 1988, MNRAS, 230, 5P

Fasano G., Franceschini A. 1988, MNRAS, 225, 155

Franceschini, A., La Franca, F., Cristiani, S., Mirones, J.M. 1994, MNRAS, 269, 683

Francis P.J., Hewett P.C., Foltz C.B., Chaffee F.H., Weymann R.J., and Morris S.L. 1991, ApJ, 373, 465

Francis P.J. 1993, ApJ, 407, 519

Giallongo E., Vagnetti F. 1992, ApJ, 396, 411

Goldschmidt P., Miller L., La Franca F., Cristiani S. 1992, MNRAS, 256, 65p

Goldschmidt P. 1994, PhD Thesis, Department of Astronomy, University of Edinburgh

Green R.F., Schmidt M., Liebert J. 1986, ApJS, 61, 305

Gunn J., Weinberg D. 1995, in Wide Field Spectroscopy and the Distant Universe, Proc. of 35th Herstmonceux Conference, ed. Maddox and Aragón-Salamanca (World Scientific, Singapore), p. 3

Haardt F., Madau P. 1996, ApJ, 461, 20

Haehnelt M.G., Rees M.J. 1993, MNRAS, 263, 168

Hartwick F.D.A., Schade D. 1990, ARA&A, 28, 437

Hawkins M.R.S., Véron P. 1995, MNRAS, 275, 1102

Hewett P.C., Foltz C.B., Chaffee F.H. 1993, ApJ, 406, L43

Hewett P.C., Foltz C.B. 1994, PASP, 106, 113

Hewett P.C., Foltz C.B., Chaffee F.H. 1995, AJ, 109, 1498

Hooper E.J., Impey C., Foltz C., Hewett P. 1995, ApJ, 445, 62

Jones L.R., McHardy I.M., Merrifield M.R., *et al.* 1996, MNRAS, in press (astro-ph/9610124)

Köhler T. 1996, PhD Thesis, University of Hamburgh

Kron, R.G. 1980, ApJ, 43, 305

La Franca F., Cristiani S., Barbieri C. 1992, AJ, 103, 1062

La Franca F., Gregorini L., Cristiani S., de Ruiter H., Owen F. 1994, AJ, 108, 1548

La Franca F., Franceschini A., Cristiani S., Vio R. 1995, A&A, 299, 19

Maccacaro T., Della Ceca R., Gioa I., Morris S., Stocke J., Wolter A. 1991, ApJ, 374, 117

Madau P., Ghisellini G., Fabian A.C. 1994, 270, L17

Marshall H.L., Avni Y., Tananmbaum H, Zamorani G. 1983, ApJ, 269, 35

Miller L., Peacock J.A., Mead A.R.G. 1990, MNRAS, 218, 265

Miller L., Goldschmidt P., La Franca F., Cristiani F. 1993, in Observational Cosmology, ASPC 51, eds. G. Chincarini, A. Iovino, T. Maccacaro and D. Maccagni, p. 614

Padovani P. 1993, 1993, MNRAS, 263, 461

Press W.H., Teukolsky S.A., Vetterling W.T., Flannery B.P. 1992, Numerical Recipes, Second Edition, Cambridge Univ. Press, Cambridge, 640

Sargent W.L.L.S., Steidel C.C., Boksenberg A. 1989, ApJS, 69, 703

Schmidt, M., Green, R.F. 1983, ApJ, 269, 352

Schneider D.P., van Gorkom J.H., Schmidt M., Gunn J.E. 1992, AJ, 103, 1451

Schneider D.P., Schmidt M., Gunn J.E. 1991, ApJS, 101, 2004

Visnovsky K.L., Impey C.D., Hewett P.C., Weymann R.J., Morris S.L. 1992, ApJ, 391, 560

Wampler E.J., Ponz D. 1985, ApJ, 298, 448

Warren S.J., Hewett P.C., Osmer P.S. 1994, ApJ, 421, 412

Wisotzki L., Köhler T., Groote D., Reimers D. 1996a, A&AS, 115, 227

Wisotzki L., Bade N., Engels D., Groote D., Hagen H.J., Köhler T., Reimers D. 1996b, in "Wide Field Spectroscopy", Athens, eds E. Kontizas *et al.*

Zitelli, V., Mignoli, M., Zamorani, G., Marano, B., Boyle, B.J. 1992, MNRAS, 256, 349

TABLE 1. QSO counts and surface densities.

TABLE 2. "Best fit" parameters for luminosity function models.

This 2-column preprint was prepared with the AAS LaTeX macros v4.0.

TABLE 1. QSO counts and surface densities.

Magnitude range B	N.	Density deg^{-2} 0.5 mag^{-1}
	HBQS[a]	
$15.4 - 15.9$	1	0.002
$15.9 - 16.4$	6	0.011
$16.4 - 16.9$	15	0.027
$16.9 - 17.4$	42	0.080
$17.4 - 17.9$	55	0.26
$17.9 - 18.4$	122	0.76
$18.4 - 18.9$	86	...
	EQS[b]	
$15.4 - 15.9$	2	0.006
$15.9 - 16.4$	5	0.015
$16.4 - 16.9$	1	...

Notes to Table 1.

QSOs are defined as objects having $M_B < -23$ and $0.3 < z < 2.2$ with $H_0 = 50\ Km/s/Mpc$ and $q_0 = 0.5$.

[a]This work

[b]Goldschmidt *et al.* (1992)

TABLE 2. "Best fit" parameters for luminosity function models.

Model	q_0	Φ $mag^{-1}Mpc^{-3}$	k_1	k_2	α	β	M^*	z'	χ^2 Prob. $z < 2.2$	2DKS Prob. $z < 0.6$
A [a]	0.5	6.5×10^{-7}	3.45	$\cdots$	-1.5	-3.9	-22.4	$\cdots$	0.12	0.01
B [b]	0.5	1.1×10^{-6}	3.26	$\cdots$	-1.39	-3.72	-22.3	$\cdots$	0.21	0.02
C [c]	0.5	9.8×10^{-7}	3.33	1.17	-1.45	-3.76	-22.3	0.40	0.53	0.09
D [d]	0.5	1.0×10^{-6}	3.29	$\cdots$	-1.39	-3.69	-22.4	$\cdots$	0.14	0.03
E [e]	0.5	1.1×10^{-6}	3.29	$\cdots$	-1.39	-3.72	-22.3	$\cdots$	0.18	0.02
F [f]	0.5	1.1×10^{-6}	3.27	$\cdots$	-1.38	-3.72	-22.3	$\cdots$	0.18	0.01
G [g]	0.5	8.5×10^{-7}	3.19	$\cdots$	-1.53	-3.87	-22.5	$\cdots$	0.13	0.01
H [h]	0.5	1.2×10^{-6}	3.00	$\cdots$	-1.37	-3.81	-22.4	$\cdots$	0.05	0.01
I [i]	0.1	4.5×10^{-7}	3.55	$\cdots$	-1.6	-3.8	-22.6	$\cdots$	0.004	0.01
L [l]	0.1	3.4×10^{-7}	3.44	$\cdots$	-1.57	-3.75	-22.9	$\cdots$	0.36	0.08
M [m]	0.1	4.0×10^{-7}	3.45	0.92	-1.50	-3.74	-22.8	0.40	0.49	0.11
1 σ errors:			± 0.07	± 0.27	± 0.07	± 0.13	± 0.2			

[a] PLE model from Boyle (1992) which includes a $z_{cut} = 1.9$ parameter
[b] Our best fit PLE model
[c] Our best LDLE model.
[d] PLE model without our HBQS data.
[e] PLE model without the EQS (Goldschmidt *et al.* 1992) data.
[f] PLE model without the LBQS (Hewett, Foltz and Chaffee 1995) data.
[g] PLE model with a spectral slope dispersion $\sigma_\gamma = 0.3$.
[h] PLE model with a spectral slope dispersion $\sigma_\gamma = 0.5$.
[i] PLE model from Boyle (1992) which includes a $z_{cut} = 2.1$ parameter
[l] Our best fit PLE model
[m] Our best LDLE model.